Mechanism of and Defect Formation in the Self-Assembly of Polymeric Polycation−Montmorillonite Ultrathin Films

N. A. Kotov,*,†,‡ T. Haraszti,§ L. Turi,§ G. Zavala,‡ R. E. Geer,⊥ I. Dékány,§ and J. H. Fendler*,‡

Contribution from the Department of Chemistry, University of Oklahoma, Stillwater, Oklahoma 74078, Department of Chemistry and the W. M. Keck Center for Molecular Electronics, Syracuse University, Syracuse, New York 13244-4100, Department of Colloid Chemistry, Attila József University, Szeged H-6720, Aradi V.t.1, Hungary, and Department of Physics, State University of New York at Albany, Albany, New York 12222

Received December 23, 1996[⊗]

Abstract: Positively charged polydiallyldimethylammonium chloride, P, was found to bind strongly to the surface of anionic montmorrillonite, M, platelets in aqueous dispersions up to a saturation (estimated to correspond to the binding of five P to one 1.0 nm × 200 nm M platelet) beyond which reversible physisorption occurred. Immersion of a substrate (glass, quartz, silica-wafer, gold, silver, and even Teflon) into an aqueous 1% solution of P and rinsing with ultrapure water for 10 min resulted in the strong adsorption of a 1.6 nm thick P on the substrate. Immersion of the P coated substrate into an aqueous dispersion of M and rinsing with ultrapure water for 10 min led to the adsorption of 2.5 nm thick M. Repeating the self-assembly steps of P and M for *n* number of times produced $(P/M)_n$ self-assembled films. Thickness of the M layer was found to depend on the external voltage applied during its self-assembly: applying a positive potential during the self-assembly of M increased the thickness of the M layer; application of a small negative potential decreased it slightly; however, larger negative voltages augmented it. The structure of self-assembled $(P/M)_n$ films have been characterized by a variety of techniques: X-ray diffraction, X-ray reflectivity, atomic force microscopy, transmission electron microscopic, and surface plasmon spectroscopic measurements. It was shown that clay platelets form stacks upon adsorption to the polymer layer consisting on the average two aluminosilicate sheets. The evolution of the surface roughness upon sequential deposition of P/M layers was observed by *in situ* AFM. Large etched pits, up to 700 nm diameter and 30 nm depth, were smoothed during P/M deposition. Small pits (188 nm diameter and 14 nm deep) were capped after one P/M deposition cycle. Surface roughness of $(P/M)_n$ films was estimated by a number of methods including surface plasmon spectroscopy. The overall roughness did not appear to correlate with the type of substrate used. On the other hand, application of an external electric field during the self-assembly of P strongly influenced the surface morphology. Application of a negative potential during the self-assembly of P improved the uniformity and regularity of the deposited layers.

Introduction

The self-assembly of oppositely charged polyelectrolytes and nanostructured inorganic or organic particles provide a viable colloid chemical approach to the preparation of advanced materials with desired optical, electro-optical, and electronic properties.[1−3] The pioneering layer-by-layer self-assembly of cationic and anionic colloidal particles[4] has been extended to that of oppositely charged polyelectrolytes,[5−7] polyelectrolytes and clay platelets,[8−12] polyelectrolytes and graphite oxide platelets,[13] polyelectrolytes and exfoliated zirconium phosphate platelets,[14] polyelectrolytes and colloidal metal particles,[15−17] and polyelectrolytes and semiconductor colloids.[12] Thus, the self-assembly of anionic and cationic molecules or clusters have become a recognized method for the construction of two-dimensional arrays and three-dimensional networks.[18] The method involves the adsorption of negatively charged species, from their solution or dispersion, onto a cationic surface. Subsequent to rinsing and drying the substrate, positively charged molecules (or clusters) are adsorbed, from their solution or dispersion, onto the anionic surface. Repeated adsorption,

† University of Oklahoma. E-mail: kotov@okway.okstate.edu.
‡ Syracuse University.
§ Attila József University.
⊥ State University of New York at Albany.
⊗ Abstract published in *Advance ACS Abstracts,* July 1, 1997.

(1) Fendler, J. H. Membrane-Mimetic Approach to Advanced Materials. In *Advances in Polymer Science*; Springer-Verlag: Berlin, 1994, Vol. 113.
(2) Fendler, J. H.; Meldrum, F. C. *Adv. Mater.* **1995**, *7*, 607−632.
(3) Capasso, F. *Thin Solid Films* **1992**, *216*, 59−67.
(4) Iler, R. K. *J. Colloid Interfac. Sci.* **1966**, *21*, 569−594.
(5) Decher, G.; Hong, J. D.; Schmitt, J. *Thin Solid Films* **1992**, *210/211*, 831−835.
(6) Lvov, Y.; Haas, H.; Decher, G.; Mohwald, H.; Mikhailov, A.; Mtchedlishvily, B.; Morgunova, E.; Vainshtein, B. *Langmuir* **1994**, *10*, 4232−4236.
(7) Lvov, Y.; Essler, F.; Decher, G. *J. Phys. Chem.* **1993**, *97*, 13773−13777.
(8) Kleinfeld, E. R.; Ferguson, G. S. *Chem. Mater.* **1995**, *7*, 2327−2331.
(9) Kleinfeld, E. R.; Ferguson, G. S. *Science* **1994**, *265*, 370−373.
(10) Kleinfeld, E. R.; Ferguson, G. S. *Mat. Res. Soc. Symp. Proc.* **1995**, *369*, 697−702.
(11) Lvov, Y.; Ariga, K.; Ichinose, I.; Kunitake, T. *Langmuir* **1996**, *12*, 3038−3044.
(12) Kotov, N. A.; Dékány, I.; Fendler, J. H. *J. Phys. Chem.* **1995**, *99*, 13065−13069.
(13) Kotov, N. A.; Dékány, I.; Fendler, J. H. *Adv. Mater.* **1996**, *8*, 637−641.
(14) Keller, S. W.; Kim, H. N.; Mallouk, T. E. *J. Am. Chem. Soc.* **1994**, *116*, 8817−8818.
(15) Feldheim, D. L.; Crabar, K. C.; Natan, M. J.; Mallouk, T. E., *J. Am. Chem. Soc.* **1996**, *118I*, *7640*−7641.
(16) Schmitt, J.; Decher, G.; Dressik, W. J.; Branduo, S. L. Geer, R. E.; Shashidhal, R.; Calvert, J. M. *Adv. Mater.* **1997**, *9*, 61 −65.
(17) Freeman, R. G.; Grabar, K. C.; Allison, K. J.; Bright, R. M.; Davis, J. A.; Guthrie, A. P.; Hommer, M. B.; Jackson, M. A.; Smith, P. C.; Walter, D. G.; Natan, M. J. *Science* **1995**, *267*, 1629−1632. Grabar, K. C.; Freeman, R. G.; Hommer, M. B.; Natan, M. J. *Anal. Chem.* **1995**, *67*, 735−743. Freeman, R. G.; Grabar, K. C.; Allison, K. J.; Bright, R. M.; Davis, J. A.; Guthrie, A. P.; Hommer, M. B.; Jackson, M. A.; Smith, P. C.; Walter, D. G.; Natan, M. J. *Science* **1995**, *267*, 1629−1632.
(18) Decher, G. In *Comprehensive Supramolecular Chemistry*; Sauvage, J.-P., Ed.; Elsevier: New York, 1996; Vol. 9.

S0002-7863(96)04409-5 CCC: $14.00

rinsing, and drying of oppositely charged species result in the build-up of films composed of the desired number of sandwich layers. The process is governed by a delicate balance between adsorption and desorption equilibria of species with appropriate hydrophobicities, charges, and charge densities. The efficient adsorption of one, and only one, monolayer of molecules (or monoparticulate layer of nanoparticles or platelets) onto the oppositely charged substrate surface is the objective of the immersion step. Preventing the desorption of the attached species during the rinsing process is of equal importance. Optimized self-assembly, in terms of adsorption and desorption, is an important requirement for the preparation of uniform and defect free films. This, in turn, necessitates an understanding of the thermodynamics and kinetics of self-assembly and of the structures of the self-assembled films. We have launched, therefore, a systematic investigation into the structure and mechanisms of self-assembly, defect formation, and defect remediation in self-assembled films. Attention is focused in the present report on the self-assembly of ultrathin films composed of alternating layers of polyelectrolytes and montmorillonite clay platelets.

The unique morphology have dictated selection of montmorillonite for self-assembly. In dilute (less than 0.1 wt %) dispersions the montmorillonite particles exfoliate into single sheets (or thin platelets composed of 2−3 sheets) in which the negative charge is balanced by inter- and intralamellar sodium cations. The virtue of montmorillonite sheets and platelets is that they cover large surface areas and smooth defects. Additionally, montmorillonite platelets have been used as catalysts[19] and sensors.[20] Introduction of one to three polyelectrolyte−montmorillonite sandwich layers between polyelectrolyte−titanium dioxide nanoparticle sandwich layers, self-assembled onto a working electrode, substantially reduced the photocurrent generated upon band-gap illumination, for example.[12] Diminishing of the photocurrent was the result of blocking the movements of the charge carriers by the large montmorillonite sheets laying flat on their faces on top of the polyelectrolyte layer. Furthermore, the closer a given polyelectrolyte−montmorillonite sandwich layer was placed to the electrode the more pronounced was the photocurrent reduction.[12]

Experimental Section

1. Materials. Sodium montmorillonite, M (Mad, Hungary), was purified by peptidization. Ten grams per liter was suspended in water. The suspension was allowed to settle in a 20 cm long jar for 17 h. The supernatant (containing <2 μm diameter M particles) was removed and converted to Na−M by stirring with 1.0 N NaCl. The Na−M particles were then separated by centrifugation, washed, and dialyzed to remove the excess electrolyte. Analysis: SiO_2 = 61.58%, Al_2O_3 = 22.15%, Fe_2O_3 = 4,5%, CaO = 0.14%, Na_2O = 3.18%, alkaline earth metals = 0.95%, water hydration = 8.0%; specific surface area (determined by N_2 adsorbtion at 77 K, using the BET equations) = 58 m^2/g. Basal distance in air dried M = 1.25 nm (X-ray diffraction). M dispersions were prepared by sonicating 2.0 g of purified, air-dried, Na−M in 100 mL of distilled water for 40 min. A rougher fraction was sedimented, and the supernatant was sonicated again for 20 min. After two centrifugations at 3000 rpm the top fraction was separated and used in the formation of M-polymer complexes and self-assembly.

Polydiallyldimethylammonium chloride, P (Aldrich, MW = 400 000−500 000), and polystyrene sulfonate, PS (Aldrich), were used as received.

Water was purified by a Millipore Milli-Q system containing a 0.22−μm Millistack filter at the outlet.

Quartz and glass slides film substrates were cleaned by soaking in concentrated sulfuric acid containing "Nochromix" for 0.5−3.0 h and rinsing, subsequently, by copious amounts of deionized water. Silica wafers (Virginia Semiconductor Co.) and Teflon were cleaned by sonication in chloroform for 20 min and rinsed in water. For surface plasmon spectroscopy glass substrates were coated first by chromium (1.5 ± 0.5 nm thick) and then by gold (45.0 ± 5.0 nm thick) films by sputtering. All substrates were kept in a clean dust free environment prior to their use.

2. Methods. In calculating the adsorption isotherms, the amount of P adsorbed on M was determined by using eq 1

$$n^s = V(C^0 - C^e)/m \qquad (1)$$

where n^s is the adsorbed amount of P, in (mg of P)/(g of M), V is the total volume of the P solution in cm^3, C^0 is initial concentration of P and C^e is the equilibrium concentration of P, both in (mg of P)/cm^3 solution, and m is the mass of M (in grams). The adsorption of P was measured by a static method. A series of M dispersions, each containing 0.5 g of M in 5.0 mL of water, were prepared in Teflon cap covered 20 cm^3 glass tubes by sonication. Addition of different volumes (0.5−3.0 mL) of 1.0% aqueous P (w/v) flocculated the PM complex. Subsequent to centrifugation (at 3000 rpm) the concentration of P was determined in the supernatant (= C^e) by absorption spectrophotometry (Uvicon 930, at 225 nm and using a calibration curve to convert absorbances to concentrations).

Normally, the process of self-assembly consisted of the cyclic repetition of four steps: (1) immersion of the substrate into an aqueous 1% (w/v) solution of P for 10−15 min, (2) rinsing with ultrapure water for 10 min, (3) immersion into an aqueous dispersion of M, prepared as described, for 10 min, and (4) the final rinsing with water for 10 min. No pretreatment or precoating of the substrates was found to be necessary. The following notations are employed in this work: n = number of deposition cycles (i.e., the number of repetitions of steps 1−4); the film formed as a result of n deposition cycles (involving P and M, for example) will be referred to as $(P/M)_n$; P/M-sandwich-layer or P/M-layer are used to describe a given pair of P and M layers; and P-layer or M-layer will be used to refer to a single layer of the polyelectrolyte of montmorillonite adsorbed onto the substrate.

$(P/M)_n$ films were also prepared by self-assembly under potential in a standard three-electrode electrochemical cell. Glass slides coated by 1.5 ± 0.5 nm of Cr and then by 45.0 ± 0.5 nm of Au were used as substrates. A standard calomel electrode, SCE (Orion) and a 0.25 mm Pt wire (Aldrich) served as the reference and the counter electrode, respectively. Conductivity was provided by the charged P or M; no additional supporting electrolyte was used. The substrate was connected to the bias source (EG&G PAR 273 potentiostat - galvanostat), immersed into an appropriate solution of P (or dispersion of M), and the desired potential was applied for 10−15 min. When the potential assisted self-assembly of M or P was completed, the substrate was rinsed with ultrapure water for 0.5−1 min, dried by a stream of nitrogen, and introduced into a dispersion of M (or solution of P). In a given self-assembled film only one of the components, either P or M, was assembled under a potential. Surface plasmon spectroscopy was used for the characterization of films obtained by potential assisted self-assembly.

Hydrodynamic diameters of the clay platelets in aqueous dispersions were determined by dynamic light scattering using the exponential sampling method of an RTG log−log photon correlator instrument connected to a Sematech SEM-633 stepping motor driven light scattering system. A HeNe (15 mW) laser was used as a light source. Typically, 13.0 μs samples times were used, and a given measurement took 200 s.

X-ray diffraction measurements were taken on a Phillips PW 1820 diffractometer (CuKα, λ = 0.154 nm). The basal distances were calculated from the peak positions by the Bragg equation, by using the PW 1877 automated powder diffraction program, with an accuracy of ±0.01 nm.

(19) Rozengart, M. I.; V'yunova, G. M.; Isagulyants, G. V. *Russian Chemical Rev.* **1988**, *57*, 115−128. Dékány, I.; Turi, L.; Tombácz, E.; Fendler, J. H. *Langmuir* **1995**, *11*, 2285−2292.

(20) Bard, A. J.; Mallouk, T. In *Molecular Design of Electrode Surfaces*; Murray, R. W., Ed.; John Wiley & Sons, Inc.: New York, 1992; pp 270−312. Ferguson, G. S.; Kleinfeld, E. R. *Adv. Mater.* **1995**, *7*, 414−416. Bard, A. J.; Mallouk, T. In *Molecular design of electrode surfaces*; Murray, R. W., Ed.; John Wiley & Sons, Inc.: New York, 1992; Vol. XXII, pp 270−312.

X-ray reflectivity measurements were performed on a Rigaku RU-200 rotating anode source. The X-ray beam (Cu Kα_1 radiation λ = 0.154 nm) used for diffraction was collimated by two tantalum slits placed between the sample and the monochromator (graphite) and two more between the sample and the NaI scintillation detector. The spectrometer radius is 49 cm. The in-plane resolutions are $\Delta q_x = 1.5 \times 10^{-4}$ nm^{-1} and $\Delta q_z = 2.2 \times 10^{-4}$ nm^{-1} where the *z*-axis is normal to the film surface and the *x*-axis is perpendicular to this normal and in the scattering plane. The out-of-plane resolution, $\Delta q_y = 0.02$ nm, was determined primarily by the slit height. No analyzer crystal was used. The sample was mounted such that a point on its surface coincided with the eucentric point of a Huber four-circle goniometer. At zero scattering angle the sample surface was parallel to the incident X-ray beam. Measurements were performed at room temperature.

Surface plasmon spectroscopic (SPS) measurements were carried out on a home constructed system. Gold (vacuum evaporated to 40−50 nm thickness) coated glass slides were used as the reflection element. The uncoated side of the slide was brought into optical contact with the base of a 90° glass prism ($\eta = 1.52$) by an index matching oil ($\eta = 1.518 \pm 0.0005$). P-polarized 632.8 nm beam was directed to the base of the prism by a HeNe Laser (Hughes, 3235H-PC, *ca.* 20 mW). The prism was mounted on a stepping motor driven rotator (Oriel) which was capable of synchronously varying the angle of incidence, θ, and the direction of a large area silicon detector (Newport, 818-SL) with an angle resolution of 0.01°. The angular sample interval was 0.1°. Angular reflection scans required about 5 min. Each angular scan was fitted to a theoretical reflection curve, calculated by choosing appropriate one, two, or three layer models and constant refractive indices.[21]

Atomic force microscopic, AFM, measurements were performed, in air, by using a Topometrix Explorer system equipped with a 2.6 μm scanner. The system was mounted on an optical table, floating on a nitrogen cushion. Silicon tips (force constant of 50 N/m) were used in the noncontact mode. Prior to the experiment, known samples and standards were scanned in ranges corresponding to the experiments to be performed in order to establish alignment and stability. In all the experiments, the same reduction of amplitude oscillation of the tip (50%) and the same set point in the system were used to maintain feedback. AFM allowed the layer-by-layer visualization of the self-assembly process. Self-assembly of P- and M-layers were performed *in situ* on the AFM base. Careful handling afforded the scanning of the same area subsequent to the removal of the AFM head, self-assembling a layer of P (or M) and washing. All these operations had to be done with extreme caution in order not to disturb the position of the sample on the base. With care it was possible to scan the same area with a precision of 200−400 nm. Thermal drift was the limiting factor in this approach. It was advisable to limit the head-away time to 10−20 min and adjust the position of the scanner after that to insure complete coincidence of the scanned images. Such a simple precaution as doing the AFM experiments in a clean-room environment with stable temperature can substantially decrease thermal fluctuations of the piezo element of AFM head. Up to 20 different areas on each sample were examined.

Ultrathin $(P/M)_n$ films were self-assembled *in situ* on the AFM base by the following steps. A small amount of P solution were spread onto a silicon wafer placed onto the AFM base (step 1). Subsequent to *ca.* 2 min of incubation the liquid was sucked off by a glass capillary and replaced with pure water and removed suction. This rinsing process was repeated 5−6 times (step 2). A dispersion of P was then spread over the substrate and allowed to stay thereon for 2−5 min (step 3), after which it was rinsed as described in step 2 (step 4). Repeating steps 1−4 n times lead to $(P/M)_n$.

Absorption spectra were taken on a Hewlett-Packard 8452A diode array spectrophotometer.

Results

1. Dynamic Light Scattering. The M dispersion used for self-assembly (see Materials section) was diluted 10-fold for dynamic light scattering measurements. The average diffusion coefficients were determined for two samples to be 2.47×10^{-8} and 2.39×10^{-8} cm^2/s; and using the canned program of the instrument mean hydrodynamic diameters, D_H, of 172 and 178 nm and polydispersity indices, I_P, of 0.209 and 0.234 were obtained, respectively. It should be pointed out that the assessment of D_H-values implicitly assumes spherical symmetry of the particles and that I_P is the product of polydispersity and deviation from spherical symmetry. The value of I_P for symmetrical and monodispersed particles should be less than 0.1. The relatively good I_P-values obtained for M dispersions indicate a high degree of monodispersity of the clay platelets since their morphology substantially deviate from spherical symmetry.

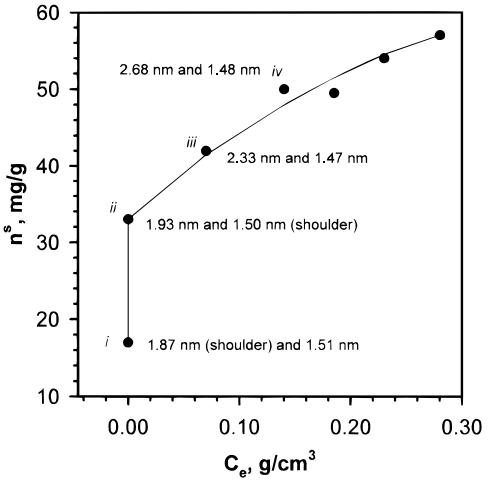

Figure 1. Adsorption isotherm of P on M in water (see Experimental Section). Points i, ii, iii, and iv correspond to P to M ratios in the polymer solution−clay dispersion for which X-ray diffraction measurements were performed. The numbers i−iv denote the characteristic spacing of X-ray diffraction peaks observed for corresponding solid samples (obtained after evaporation of the flocculated dispersions).

2. Adsorption Isotherms for the Interaction of P with M in Water. The adsorption of positively charged P on the surfaces of anionic M platelets, dispersed in water, is described by the isotherm shown in Figure 1. There are two portions of the isotherm. The first portion (the section between i and ii in Figure 1) corresponds to the ion exchange adsorption. In this region all P is adsorbed within and/or at the surfaces of M platelets, (i.e., the concentration of P in the supernatant is zero; $C^e = 0$, see eq 1). The second curvilinear portion of the adsorption isotherm (the section defined by points ii, iii, and iv in Figure 1) corresponds to the reversible physisorption of P onto the surfaces of M platelets.

3. X-ray Diffraction and Reflectivity Measurements. The X-ray diffraction pattern of self-assembled $(P/M)_n$ films is characterized by a broad peak at $2\Theta = 6.1°$ or $d_M = 1.44$ nm (Figure 2a−c, curves 1) which is quite similar to that found for the basal spacing in hydrated Na−M sheets ($d_M = 1.51$). The position of this peak was shown to depend on the degree of hydration of the Na−M sheets. Thoroughly dried Na−M revealed an X-ray diffraction peak positioned at $2\Theta = 7.01°$ and a shoulder, located $2\Theta = 5.85°$ with corresponding basal spacings of $d_M = 1.24$ nm and $d_M = 1.51$ nm. Under high ambient humidity only one peak at $2\Theta = 5.83°$, $d_M = 1.51$ nm could be observed. Ultimate hydration of the Na−M sheets occurred in aqueous dispersions where the X-ray diffraction peak appeared at $2\Theta = 5.29°$ or $d_M = 1.67$ nm (Figure 3, curve 3). This behavior corresponds nicely to the reported values for M.[22−25]

Subjecting a freshly self-assembled $(P/M)_{45}$ film to heating to 500 °C, decreased the magnitude of the peak and shifted it

(21) Sawodny, M.; Knoll, W. *Trends Polym. Sci.* **1994**, *2*, 313−323.

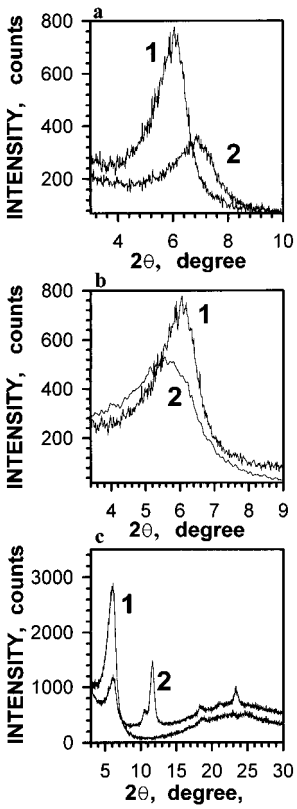

Figure 2. (a) X-ray diffraction of a $(P/M)_{45}$ film prior (curve 1) and subsequent (curve 2) heating in air to 500 °C; (b) X-ray diffraction of a $(P/M)_{18}$ film prior (curve 1) and subsequent (curve 2) to swelling in ethylene glycol; (c) X-ray diffraction of a $(P/M)_{18}$ film (curve 1) and a $(H/M)_{20}$ film (curve 2) assembled according to R. K. Iler,[4] where H = positively charged platelets of hydrotalcite.

to $2\Theta = 6.86°$ or $d_M = 1.29$ nm in accord with the expected dehydration (Figure 2a). Swelling of alumosilicate sheets by ethyleneglycol molecules have also manifested itself in shifts of the X-ray diffraction peak toward smaller angles (from $2\Theta = 6.18°$, $d_M = 1.43$ nm, to $2\Theta = 5.80°$, $d_M = 1.52$ nm (Figure 2b).[26] When a positively charged P are replaced by a similarly charged hydrotalcite sheets (Figure 2c), the position of the peak at $2\Theta = 6.2°$ remained unchanged, while a series of new peaks appeared at $2\Theta = 10-23°$. The latter corresponded to characteristic pattern of hydrotalcite. X-ray diffraction patterns of air-dried solids obtained after evaporation of polymer-clay flocculated dispersions revealed a reflection at $2\Theta = 5.85°$ ($d_M = 1.51-1.47$ nm) corresponding to hydrated M which can be seen for all concentrations of P. At low polyelectrolyte concentration a shoulder at $2\Theta = 4.72°$ ($d = 1.87$ nm) was observed. Addition of increasing amounts of P resulted in enhanced accumulation of polymer between alumosilicate sheets which manifested itself in decreasing 2Θ values and hence in increasing basal spacing: 1.93, 2.33, and 2.68 nm.

X-ray reflectivity measurements were made on films consisting of 20, 15, 10, and 4 deposition cycles (Figure 3). With the exception of the $n = 10$ film all were deposited on polished silicon wafers (100). The $n = 10$ multilayer was deposited on a glass microscope slide. The most prominent features of the specular scans (q_z-scans) are the harmonics at $2q = 6.1°$, 18.4°,

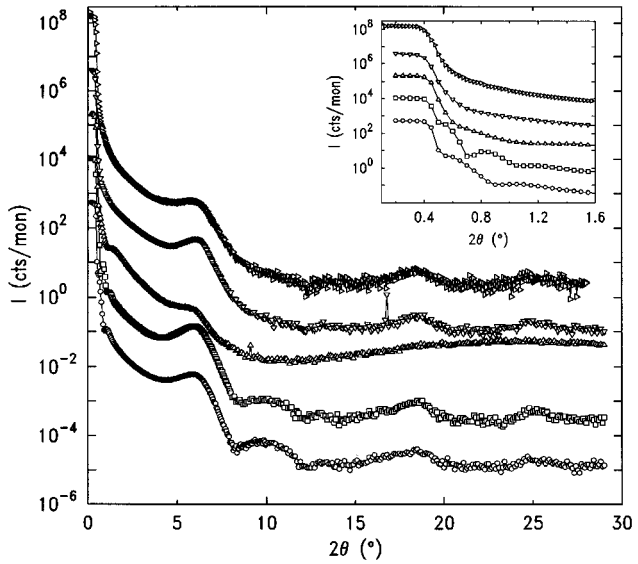

Figure 3. Specular scattering from $n = 4$ (bottom), $n = 7$, $n = 10$, $n = 15$, and $n = 20$ (top). The (001), (003), and (004) reflections from the basal spacing of the montmorillonite are evident for all thicknesses with the exception of $n = 10$ which was deposited on a glass slide and only displays the (001) reflection. The broad, high-angle scattering in the latter presumably obscure the higher order peaks. Inset shows detail at low angle for all five film thicknesses. Data are in the same relative order as in the main figure. The critical angle is evident at 0.41 degrees for all data. For $n = 7$ and $n = 4$ Kiessig fringes can be seen. These fringes damp out very quickly implying a roughness on the order of the layer spacing.

and 24.8° seen in those films on polished silicon (Figure 3). These peaks correspond to the fundamental, third and fourth-order reflections from the basal spacing of the montmorillonite particles.[27] Although the fundamental reflection is evident for the sample deposited on the glass slide, the higher order peaks are absent, most likely concealed by the broad high angle scattering due the amorphous nature of the glass.

The insert in Figure 3 shows the low angle scattering for the same samples. The critical angle associated with the substrate is clearly evident at $2q = 0.41.°$ Note that low angle Kiessig fringes corresponding to the film thickness are only evident for the $n = 4$ and $n = 7$ films. The width of the oscillations $= 2p/D$ where D is the thickness of the film.[28] The data from the inset yields thicknesses of the $n = 4$ and $n = 7$ films of 22 ± 4 and 32 ± 4 nm, respectively. The rapid decay in the oscillation amplitude is responsible for the large error bars. No hint of such oscillations can be seen in thicker films which implies that the average roughness may be increasing with film thickness, a fact which is supported by the specular diffuse scattering and rocking curves.[28]

Figure 4a shows specular and off-specular scans of the $n = 7$ film. The off-specular scan follows a trajectory $w = (q-2q/2) = 0.3°$. This places the off-specular scan parallel to but offset (in the q_x direction) from the specular data. Both specular and off-specular scans possess a peak which corresponds to the fundamental reflection of the montmorillonite particles ($2q = 6.1°$). Also present in the specular scan is a smaller peak centered at $2q = 10°$. However, as evident in Figure 4a, this peak is not present in the off-specular scan. A similar situation exists for the $n = 4$ film. Figure 4b represents the dependence

(22) van Olphen, H. *An Introduction to Clay Colloid Chemistry*; Wiley: New York, 1977.
(23) Norris, K. *Discuss. Faraday Soc.* **1954**, *18*, 120.
(24) Lagaly, G.; Weiss, A. *Angew. Chem.* **1971**, *83*, 580.
(25) Dékány, I.; Szántó, F.; Weiss, A.; Lagaly, G. *Ber. Bunsenges. Phys. Chem.* **1985**, *89*, 62−67.
(26) Newman, A. C. *Chemistry of Clays and Clay Minerals*; Mineralogical Society: London, 1987.
(27) *Crystal Structures of Clay Minerals and their X-ray Diffraction*; Brindley, G. W., Brown, G., Eds.; Mineral Society: Monograph 5, London, 1980.
(28) Geer, R. E.; Qadri, S. B.; Shashidhar, R. *Ferroelectrics* **1993**, *149*, 147. Entin, I., Goffer, R.; Davidov, D., Hersht, I. *Phys. Rev. B* **1993,** *47*, 8265.

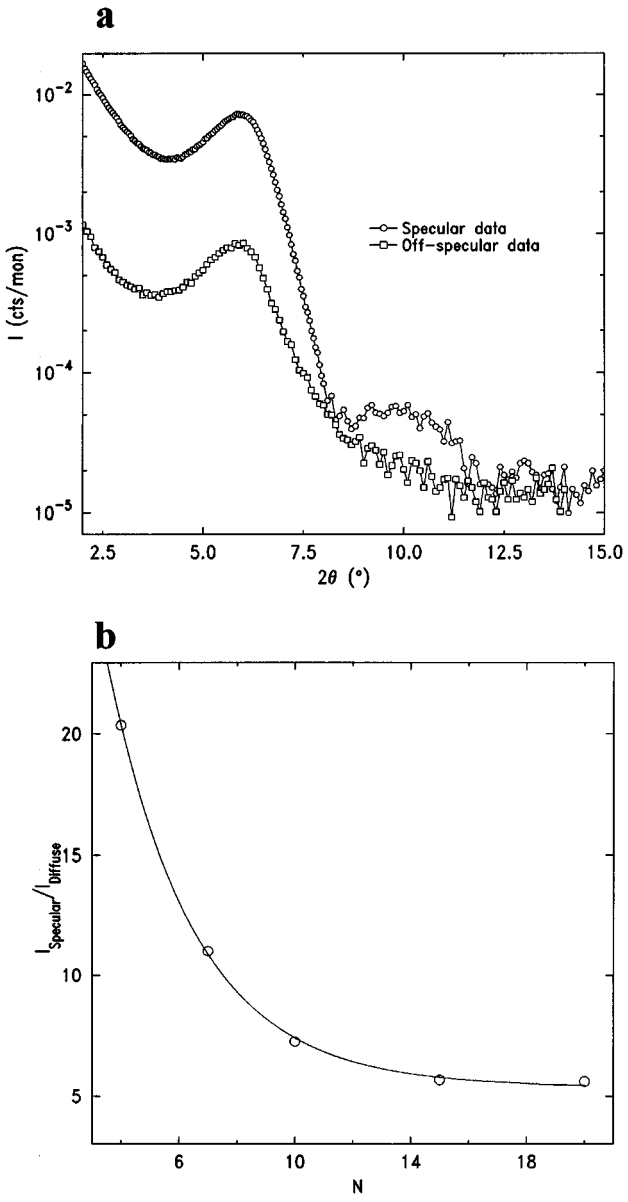

Figure 4. (a) Specular (open circles) and off-specular (open squares) X-ray reflectivity data for the $n = 7$ film. Note that the broad peak at 10 degrees seen in the specular scan is absent in the off-specular data; however, both display a peak associated with the clay particles. (b) Ratio of specular scattering to diffuse scattering at the (001) reflection from the montmorillonite particles. The solid line is a fit to a simple exponential decay. This decay implies a rms layer roughness which is damped at the surface (see text). The decay length for this damping is approximately three layers.

of the ratio of specular scattering to diffuse scattering on the number of layers. The implications of this feature are presented in the Discussion section part 3.

4. Surface Plasmon Spectroscopy. Sequential, layer-by-layer self-assembly sandwich layers of P/M films were monitored by SPS (Figure 5a). The experimentally observed angle dependence of the reflected light intensities were fitted by the Fresnel equations using available refraction indices for P and M ($\eta_P = 1.625$[29] and $\eta_M = 1.57$[30]).[31] The average thickness of a P layer was determined to be 1.6 ± 0.4 nm, while that of the M layer was 2.46 ± 0.5 nm. Thus, the mean thickness of one sandwich P/M unit was found to be 3.9 ± 0.5 nm.

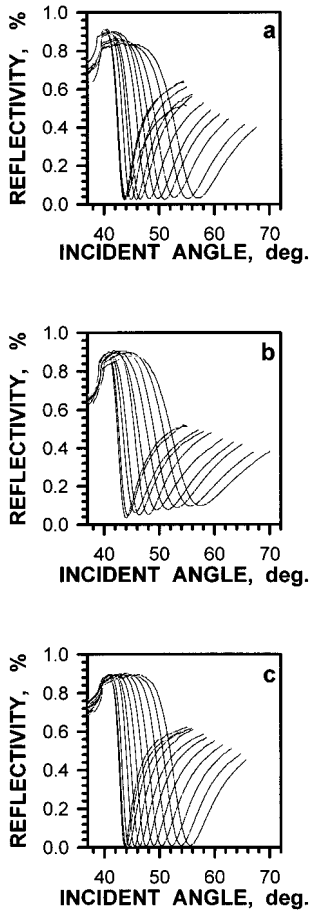

Figure 5. SPS curves for a series of sequentially deposited $(PM)_n$ films, taken after each M layer. The films were self-assembled under normal condition (a) and in the presence of a +0.6 V (b) and −2.0 V (c) potential (vs SCE) applied during the self-assembly of P. The lines were fitted by using the following dielectric constants $\epsilon_{Cr} = -6.500$ $\epsilon'_{Cr} = 0.698$; $\epsilon_{Au} = -10.954$ $\epsilon'_{Au} = 2.360$; $\epsilon_P = 2.640$ $\epsilon'_P = 0$; and $\epsilon_M = 2.470$ $\epsilon'_M = 0$ and gave $d_{(P/M)} = 3.1$, 4.1, and 2.8 nm for a, b, and c, respectively.

SPS provided a convenient means for monitoring structural changes in the self-assembled films as functions of the experimental conditions employed during the adsorption of each layer onto the substrate. For example, application of a small external voltage during self-assembly substantially altered the thickness of the film formed (Figures 5 (parts b, c) and 6). In one set of experiments potential was applied only during the self-assembly of the M platelets (Figure 6). The samples were rinsed by water for 30 s, and then self-assembly of P was performed as usual (in the absence of an applied potential). Application of a positive voltage during the self-assembly of M (Figure 6) increased of thickness of M from 2.8 ± 0.3 to 4.8 ± 0.3 nm and application of a small negative potential decreased it slightly; however, larger negative voltages augmented the thickness of M. In a separate set of experiments potential was applied during the self-assembly of P (Figure 5 (parts b, c)), while all other steps (rinsing for 30 s and self-assembly of M) were performed in the absence of bias potential. The obtained SPS results, interpreted in terms of a simple model relating to surface roughness changes, will be detailed in the Discussion section.

(29) Ramsden, J. J.; Lvov, Yu., M.; Decher, G. *Thin Solid Films* **1995**, *254*, 246−251.

(30) CRC Handbook of Chemistry and Physics, 64th ed.; CRC Press: Boca Raton, FL, 1984; B-197.

(31) Cowen, S.; Sambles, J. R. *J. Opt. Commun.* **1990**, *79*, 427. Reiter, H.; Motschmann, H.; Orenda, H.; Nemetz, A.; Knoll, W. *Langmuir* **1992**, *8*, 1784. Aust, E. F.; Ito, S.; Berreman, D. W.; Scheffer, T. J. *Phys. Rev. Lett.* **1970**, *25*, 577. Kovacs, G. In *Electromagnetic Surface Modes*; Boardman, A. D., Ed.; John Willey & Sons: New York, 1982; pp 143−200.

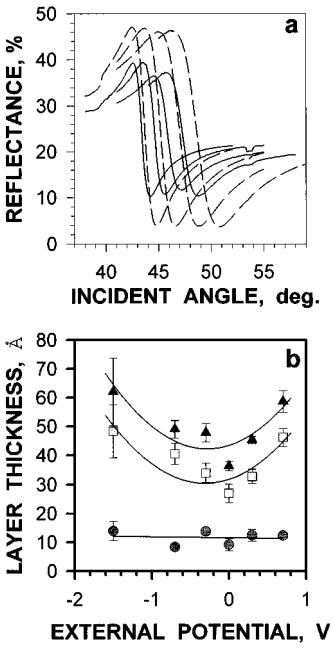

Figure 6. (a) SPS curves for a series of sequentially deposited $(PM)_n$ films, taken after each M layer, in the presence a +0.7 V (broken lines) and −0.7 V (solid lines) potential (vs SCE*)* applied during the self-assembly of M. (b) A plot of average thicknesses, determined by SPS, of the P (●), M (■), and the P/M (▲) layers vs the potential applied during the self-assembly.

5. Absorption Spectra. Absorption spectra of self-assembled $(P/M)_n$ films were routinely taken to establish the uniformity of the thickness of each adsorbed layer. In general, good linearities were observed for plots of absorbances, at a given wavelength, vs n up to $n = 20$. For thicker samples these plots showed some deviation from linearity.

6. AFM Images. Prior to self-assembly the silicon substrates were routinely imaged by AFM. The mean roughness (i.e., the average surface height variations, rms) of the substrate (Figure 7a) was found to be 0.5 nm. Upon assembly of a (P/M) layer the mean roughness increased to 5 nm (see Figure 7b). Increasing the resolution of the image permitted the visualization of the individual M platelets (Figure 7c). They appear to be somewhat irregularly shaped, with mean length of 100 nm. The line profile (Figure 7d) and height analyses over a $2.6\mu \times 2.6\mu$ area revealed a mean height of 2.5 nm for M which coincides well with the SPS data on the thickness of an M layer. Thus most M platelets are lying flat and oriented normal to the substrate, and there are, on the average, two sheets of 1.0 nm thick M platelets stacked upon P. The absence of completely flat portions in Figure 7 is the consequence of the high flexibility of the aluminosilicate sheets and of the partial image distortion by the AFM tip effects.

Typical AFM images of P/N films self-assembled on *rough* silicon substrates are shown in Figure 8. Gentle etching by HF resulted in formation of pits on the substrate surface in sizes varying from 180 to 550 nm and in depth varying from 14 to 130 nm (Figure 8). Self-assembly of one (P/M) layer was found to be sufficient to coat a 188 nm diameter pit (compare Figure 8 (parts a and c)). The identities of the circled areas in Figure 8 (parts a and c) were verified by the observation of a characteristic sequence of surface features. Covering larger pits required the self-assembly of several (P/M) layers. For example, the results of $(P/M)_6$ eliminated a 550 nm diameter wide and 50 nm deep pit. A similar effect was observed on self-assembling $(P/M)_n$ films on NaOH etched Si surfaces.

Discussion

1. Interactions of Negatively Charged Montmorillonite (M) Dispersions and Cationic Polyelectrolyte (P) Solutions in Water. Montmorillonite, M, is a smectite 2:1 clay mineral; each of its 1.0 ± 0.2 nm thick and 50−300 nm by 50−300 nm long layer is composed of an Al-octahedral sheet that shares oxygen atoms with two Si-tetrahedral sheets.[22,26,27] Substitution of other cations present in the layer (Mg^{2+}, Fe^{2+}, Li^{+}, for example) for Al^{3+} leaves an excess negative charge which is compensated by Na^{+}. The interlayer distance, referred to as basal or d(001) spacing, very much depends on the extent of hydration of the exchangeable cations, on the composition of the solvent, and on the temperature. The basal spacing for M is in the range of 0.9−3.5 nm.

When dispersed in water montmorillonite exfoliates into separate platelets. The average diameter of clay platelets, determined by light scattering, was found to be 175 ± 20 nm which corresponds to the diameter of a single platelet. The increase of clay concentration or ionic strength prompted formation of parallel stacks of platelets as well as face-to-edge and edge-to-edge agglomerates. This process may occur with or without flocculation of the dispersion. Stacking, a very characteristic property of clays, results from strong both van der Waals and dipole−dipole interaction between the sheets, where areas of partial positive charge (metal ions, Al, Si) alternate with partial negative charge (oxygen). Due to crystallinity of the alumosilicate surface they form overlapping structures where the platelets orient themselves *versus* each other to maximize the dipole−dipole interaction between regularly alternating spots. It is important to note that attraction forces between alumosilicate platelets act at a short distance (1−3 nm) while long-range electrostatic repulsion due to overall negative charge dominates at larger separation.

Poly(dimethyldiallylammonium) bromide (P) is a highly charged polyelectrolyte which undergoes efficient dissociation in aqueous solutions. Strong electrostatic repulsion between the positive charges on different segments of the chain results in a quite loose conformation in water. Partial coiling of P occurs only at high ionic strength owing to shielding effect of the ionic atmosphere. Predominantly linear conformation of the polyelectrolyte causes extended interchain interactions. The balance of electrostatic repulsion and hydrophobic attraction forces between hydrocarbon parts of the chain result in a partial networking of the polyelectrolyte chains.

When M sheets and P molecules are brought into the contact, an immediate flocculation of the alumosilicate dispersion occurs due to interaction between oppositely charged groups and to various short-range forces. Flocculation of polyelectrolytes and clays have produced some interesting materials with unique physical properties and high environmental stabilities.[32−35]

The inflection point on the plot in Figure 1 indicates that the mechanism of adsorption changes as the amount of polyelectrolyte increases. Initially, P binds strongly and irreversibly until the negative charge of alumosilicate platelets is practically compensated; no free polyelectrolyte is present in the solution. The saturation of the initial stage of adsorption occurs at 33 mg/g polymer/clay ratio. Assuming the molecular weight of P to be 450 000, the thickness of a platelet to be 1.0 nm, and the sides of a platelet to be 200 nm we estimate that ca. 5 polymer chains are (**) associated with an average montmorillonite

(32) Pinnavaia, T. J. *Science* **1983**, *220*, 365−369.
(33) Lan, T.; Pinnavaia, J. T. *Chem. Mater.* **1994**, *6*, 2216−2219.
(34) Biasci, L.; Aglietto, M.; Ruggeri, G.; Ciardelli, F. *Polymer* **1994**, *35*, 3296−3303.
(35) Biasci, L.; Aglietto, M.; Ruggeri, G.; Dalessio, A. *Polym. Adv. Technol.* **1995**, *6*, 662−670.

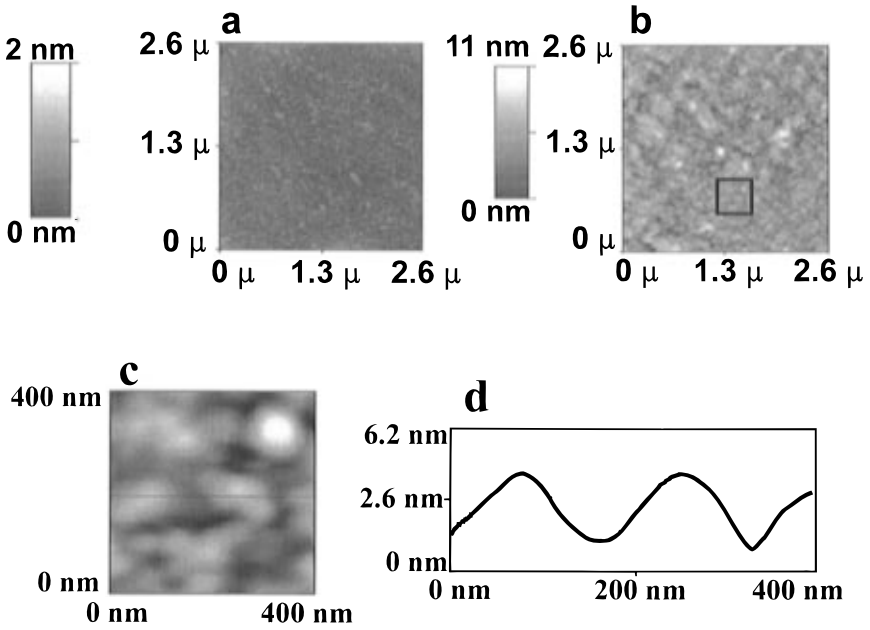

Figure 7. Typical AFM image of a bare silicon wafer substrate prior (a) and subsequent to the self-assembly of a (P/M) layer onto it (b and c). The silicon wafer was scanned in different positions, and the images obtained were virtually identical to the image presented. Special care was taken to image the very same areas prior (a) and subsequent to the self-assembly of a (P/M) layer (see Experimental Section). The AFM image shown in b was representative of the whole wafer since very similar images were obtained by scanning five different spots which were located 0.5 cm from each other. AFM image shown in c was obtained by zooming-in the area highlighted by square in b. The profile of the line indicated by the horizontal line in c is drawn in d. The mean difference between the minima and maxima in the line profile, 2.0 ± 0.2 nm, corresponds to the thickness of the M layer in the (P/M) film.

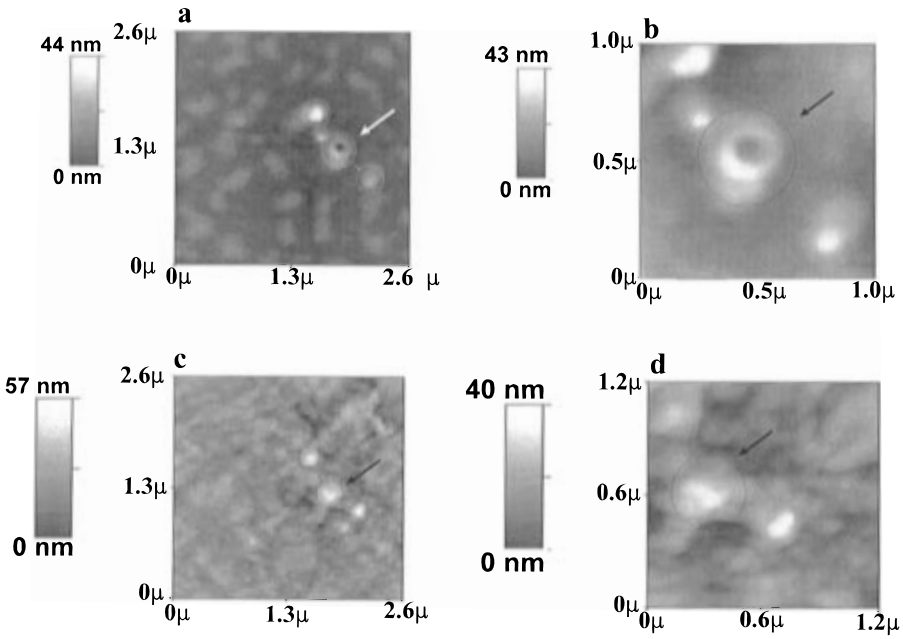

Figure 8. Typical AFM images of volcanic-crater-shaped pits seen in HF-etched silicon wafer surfaces at a lower (a) and higher (b) resolution. The crater presented here is seen to have a diameter of 188 nm and a depth of 14 nm. The same areas are imaged subsequent to the *in situ* self-assembly of a (P/M) layer (see Experimental Section) at a lower (c) and higher (d) resolution. Identities of the areas a and c and b and d were verified by the observation of characteristic sequence of surface features (see the three circled areas in all four images). Interestingly, the hollow region of the pit can no longer be observed after the self-assembling of a (P/M) layer onto it. Apparently, the craters were capped by clay platelets.

sheet.[36] The subsequent curvilinear portion of the adsorption isotherm defines the reversible physisorption of P onto the surfaces of M platelets. Importantly, thus associated polymer can be easily removed from the surface of alumosilicate sheets by dilution or by washing.

The effect of increasing the amount of P incorporated into the M matrix (from the dispersion by flocculation) can be seen also from X-ray diffraction data. For small P/M ratio (point i in Figure 1) when irreversible adsorption takes place, the basal spacing of M does not change appreciably. The diameter of the hydrocarbon chain (<4 Å) allows the incorporation of P

(36) Taking 1 nm to be the thickness and 200 nm to be the sides of a montmorillonite platelet, we calculate that their elementary volume is 4×10^{-17} cm^3. Further, using an average density of 2.8 g/cm^3 for M we calculate that there are 9×10^{15} platelets in 1 g of M. Taking 450 000 for the molecular weight of P we estimate that there are 4.4×10^{16} chains of P present in 33 mg which is bound to 1.0 g of M. Thus the ratio of the number of P to the number of M platelet is 4.9 or 5. These calculations should be considered, of course, to be highly approximate.

into the regular clay layered structure. A shoulder peak appears at 1.87 nm which corresponds to a new phase where several layers of P are penetrated between clay sheets and "wedged" the basal spacing. This process progresses as the concentration M increases. The shoulder of a thick-P-layer phase grows and shifts to smaller angles. Upon addition of P one can observe the expansion of the basal spacing from 1.87 to 2.68 Å (point iv, Figure 1). Obviously, both chemi- and physisorbed polymer chains are present in this layer. Due to the high molecular weight, it is most likely that every incorporated P molecule was partially involved in both sorption mechanisms. Importantly, even at high concentration of P the basal spacing of M remains observable in the X-ray diffraction (point iv, Figure 1) indicating that M tends to flocculate not as separate platelets but as stacks. This phenomenon is important for understanding the mechanism of formation and the structure of P/M self-assembled layers.

2. Substrates for Self-Assembly. A significant contribution of the present work is the demonstration that oppositely charged P and M (or any other particles) can self-assemble on virtually any kind of clean substrate. Pretreatment of the substrate, by heating in an oxidizing atmosphere or by grafting an organic molecule on the surface, was routinely performed in previously reported procedures for the layer-by-layer self-assembly of polyelectrolytes,[38] proteins,[39,40] and nanoparticles.[17] In the present study M and P layers were effectively assembled on most native surfaces including glass, quartz, silicon, gold, silver, and other metals without any pretreatment and without effecting the structure of the films formed. For instance, the thickness of a P layer in $(P/M)_n$ reached its characteristic value $D_P = 1.8 \pm 0.5$ nm at the second deposition cycle upon self-assembly on a gold substrate. On highly hydrophobic surfaces, such as Teflon or sililated quartz, 5−6 deposition cycles were normally necessary to obtain a constant layer thickness for each consecutive deposition.

Several factors are believed to contribute to the successful self-assembly of $(P/M)_n$ on untreated surfaces. First, there is a high affinity of polyelectrolytes to most surfaces. Indeed, various polyelectrolytes were shown to adsorb on glass,[41] plastic,[42] ceramics,[43] and other solid surfaces by a combination of hydrophobic, dipole−dipole, and ion−dipole interactions.[44] Second, the M platelets are able to cover relatively large areas which may contain defects and/or pin holes (see subsequent discussion).

The kinetics of adsorption and desorption of P (and M) play a key role in overall adhesion of the $(P/M)_n$ film to a substrate. The P layer remaining on the substrate subsequent to rinsing may not necessarily be in equilibrium with the surrounding media due to long desorption times of the high molecular weight polymers.[45] Consequently, P may not have sufficient time to desorb prior to the adsorption of the next M layer. Additionally, the alumosilicate sheets of M cement the first adsorbed P layer rendering it kinetically and thermodynamically stable, which further decreases the influence of a substrate material on the multilayer.

3. Structure and Mechanism of the $(P/M)_n$ Film Self-Assembly. The formation of stable $(P/M)_n$ films is governed by a delicate balance between adsorption and desorption driven by electrostatic and van der Waals interactions of the oppositely charge P and M. Due care needs to be exercised, therefore, in selecting P with appropriate hydrophobic−hydrophilic balance, molecular weight, surface charge, and charge density.

As was mentioned, the rate of P adsorption and desorption is an important factor determining the structure of the films. The unique morphology of M platelets also contribute to the uniformity of the $(P/M)_n$ films. They can be pictured as large irregularly cut sheets (with average diameter of 400 nm and thickness of 1 nm) with a high degree of flexibility. Defects on a P layer can be fully or partially covered by the large M platelets which provides a smooth and highly charged surface for the adsorption of the subsequent P layer. There remain, however, subtle substrate depended effects on the self-assembly.

Ultrathin films, produced by sequential self-assembly of cationic and anionic polyelectrolytes, $(P^+/P^-)_n$, were demonstrated to be smooth and to have uniformly increase their thicknesses with increasing n.[18] At the same time, the highly flexible individual P^+ and P^- layers were found to be strongly interdigitated. One might anticipate that the platelets of M may diminish interlayer mixing and promote ordering in the $(P/M)_n$ films.

X-ray diffraction revealed several broad peaks in the region of $2\theta = 4-30°$ (Figures 2 and 3). The strongest one is located at $2\theta = 6.2°$. This peak is identical to the basal spacing reflection of M, observed both in the neat and P flocculated clay. The positive and negative shifts of the peak are due to dehydration at elevated temperatures (Figure 2a) and swelling in ethyleneglycol (Figure 2b), respectively. This behavior corresponds to that expected.[26] On the other hand, the position of the $2\theta = 6.2°$ peak remained unchanged in films with different multilayer structures as long as M was one of the components (Figure 2c). An increase of the ionic strength of the P solution was previously shown to lead to thicker polymer layers.[18] Although the $2\theta = 6.2°$ peak for $(P/M)_n$ films assembled in 0.1 M NaCl became slightly broader, it did not change the position. The same was observed for a film composed from M and positively charged layered alumosilicate, hydrotalcite (Figure 2c) assembled following R. K. Iler's method.[4] Thus, the experimental results warranted the attribution of this peak to the interplatelet basal spacing rather than to interlayer spacing ($D_P + D_M$) or to a new clay-polymer crystalline phase.[46]

The structure of multilayers made of exfoliated materials and polyelectrolytes has been under consideration in several previous

(37) Ulman, A. *An Introduction to Ultrathin Organic Films, From Langmuir-Blodgett to Self-Assembly*; Academic Press: Boston, 1991.

(38) Lvov, Y.; Haas, H.; Decher, G.; Mohwald, H.; Mikhailov, A.; Mtchedlishvily, B.; Morgunova, E.; Vainshtein, B. *Langmuir* **1994**, *10*, 4232−4236. Hong, J. D.; Lowack, K.; Schmitt, J.; Decher, G. *Prog. Colloid Polym. Sci.* **1993**, *93*, 98−102, and references therein.

(39) Decher, G.; Lehr, B.; Lowack, K.; Lvov, Y.; Schmitt, J. *Biosensors Bioelectronics* **1994**, *9*, 677−684. Hong, J. D.; Lowack, K.; Schmitt, J.; Decher, G.; Laggner, P. G. O. E. *Prog. Colloid Polym. Sci.* **1993**, 98.

(40) Sano, M.; Lvov, Y.; Kunitake, T. *Annu. Rev. Mater. Sci.* **1996**, *26*, 153−187.

(41) Cosgrove, T.; Richards, R. D. C.; Semlyen, J. A.; Webster, J. R. P. In *Colloid-Polymer Interactions, Particulate, Amphiphilic, and Biological Surfaces*; Dubin, P., Tong, P., Eds.; ACS Symposium Series, American Chemical Society: Washington, DC, 1993; p 111.

(42) Wesslen, B.; Kober, M.; Freijlarsson, C.; Ljungh, A.; Paulsson, M. *Biomaterials* **1994**, 15, 278−284. Abel, M. L.; Chehimi, M. M.; Brown, A. M.; Leadley, S. R.; Watts, J. F. *J. Mater.* **1995**, *5*, 845−848. Noinville, V.; Vidalmadjar, C.; Sebille, B. *J. Phys. Chem.* **1995**, *99*, 1516−1522.

(43) Bjorklund, R. B.; Arwin, H.; Jarnstrom, L. *Appl. Surf. Sci.* **1994**, *75*, 197−203. Filippov, L. K.; Silebi, C. A.; Elaasser, M. S. *Langmuir* **1995**, *11*, 872−879. Kawaguchi, M.; Naka, R.; Imai, M.; Kato, T. *Langmuir* **1995**, *11*, 4323−4327. Dijt, J. C.; Cohen Stuart, M. A.; Fleer, G. J. In *Coloid-Polymer Interactions, Particulate, Amphiphilic, and Biological Surfaces*; Dubin, P., Tong, P., Eds.; ACS Symposium Series, American Chemical Society: Washington, DC, 1993; p 14.

(44) Ploehn, H. J. Self-Consistent-Field Theory for Polymer Adsorption - Molecular Volume Effects. *Colloids Surf. A* **1994**, *86*, 25−40. Vongoeler, F.; Muthukumar, M. *J. Chem. Phys.* **1994**, *100*, 7796−7803. Vanderlinden, C. C.; Vanlent, B.; Leermakers, F. A. M.; Fleer, G. J. *Macromolecules* **1994**, *27*, 1915−1921.

(45) Xu, H.; Schlenoff, J. B. *Langmuir* **1994**, *10*, 241−245. Lipatov, Y.; Todosijchuk, T.; Chornaya, V. *J. Colloid Interfac. Sci.* **1995**, *174*, 361−367. Wang, W. P.; Barton, S. W. *J. Phys. Chem.* **1995**, *99*, 2845−2853. Vandeven, T. G. M. *Adv. Colloid Interfac. Sci.* **1994**, *48*, 121−140.

publications.[9−11,13,14] The important fact that has been established for such systems is the linear increase of film thickness during the deposition. Therefore, the films obtained by the sequential adsorption of oppositely charged compounds indeed represent a rather regular structure. Nonetheless, a degree of order obtained in such films as well as the means to improve it are still to be determined. The AFM and SEM data published by several groups for the same or analogous layer-by-layer systems[9−11,13−15] suggest that the roughness of a layer of inorganic materials adsorbed to a polymer is higher than that of polyelectrolyte layers.[18] In fact, it exceeds the average thickness of both individual polymer and clay films. This factor has not been taken into account when discussing the structure of clay-polyelectrolyte multilayers yet. As we shall show below considering the roughness parameter is critical for the interpretation of the X-ray diffraction pattern of such films and provides important insights in the mechanism of their formation.

The thickness of a P/M film, deposited in one cycle, $D_{P/M}$, was found to be 3.9 ± 0.5 nm by SPS. This value is in a good agreement with that obtained from the Kiessig fringes in the X-ray diffraction measurements, 4 ± 0.5 nm (Figure 5 insert) for $(P/M)_7$. In similar systems a one-cycle thickness increment was reported to be $D_{P/M} = 3.6 \pm 0.4$,[11] and 3.2−3.8 nm.[9] Evidently, there is little variation in the thickness of P/M layers deposited in one cycle. Nevertheless, the dimensions of individual P and M layers vary rather substantially. The Japanese group reported D_P and D_M to be 2.2 and 1.4 nm, respectively[11] implying some intercalation of M and P. Klein and Ferguson reported much smaller D_P and D_M values (0.5 and 1.0 nm, respectively).[9] They rationalized the discrepancy between the total layer thickness (3.8 nm) and the sum of a P and M layer ($D_P + D_M = 1.5$ nm) by assuming the deposition of two P/M units during one deposition cycle. The SPS results, obtained in the present work ($D_P = 1.6 \pm 0.4$ nm and $D_M = 2.4 \pm 0.5$ nm), corresponded to an average of 1.7 M platelets. Greater than unity number of platelets in the clay film is likely to reflect the difficulty of the complete neutralization of the surface charge on P with one layer of *irregular* M sheets. The observation of the basal spacing reflection in the X-ray diffraction pattern also supports the fact that the M layer is formed by short stacks of platelets rather than from completely exfoliated sheets interlaced with polymer. We believe that the structure of multilayers can be pictured by a simplified scheme in Figure 9a. Importantly, the surface profile taken by zooming in on flat parts of the film's surface reveal remarkable similarity to Figure 7d. The AFM images (Figures 7b and 8a) also revealed overlapping clay platelets within an M layer. Note that stacking of clay platelets and, hence, increased roughness of the film surface resulted in such a broadening of the diffraction originating in the (P/M) repeating units that this diffraction (expected at $2\theta \approx 2°$ corresponding to $D_{P/M} = 4$ nm) could hardly be observed.

Due to stacking the difference in the size of individual platelets may translate into a thickness variation of the M layer. The larger the M sheet is, for example, the wider area can be covered by a single layer of M platelet without exposing the underlaying P layer. Y. Lvov, T. Kunitake, and co-workers used ca. 500 nm M particles,[11] whereas in our study the size of individual platelets was around 150 nm. This difference resulted in a thickness variation of the M layer; $D_M = 1.4$ nm for the larger sheets,[11] and $D_M = 2.4$ nm for the smaller ones used by us. Note that both values exceeded the thickness of a single M sheet (0.95 nm).

Interestingly, the thickness of both clay and polyelectrolyte layers can be changed by applying an external voltage during the self-assembly. The thickness of the M layer was found to increase from 2.4 ± 0.3 to 4.8 ± 0.3 nm by changing the bias from 0.0 to +0.7 V during the self-assembly of M (Figure 6 (parts a and b)). This effect is primarily connected with the attraction of the negatively charged M platelets to the positively charged electrode (and to positively charged P). Since no potential was applied during the rinsing, reestablishment of the equilibrium density of M particles on the surface is the *a priori* expectation. Indeed this is what happened if prolonged (>30 min) rinsing times were employed. However, rinsing the $(P/M)_n$ films for times shorter (0.5 min) than that required for the exfoliation M and conformational changes of P (in the order of 15−20 min) retained the bias potential induced thickness changes. This, of course, is the consequence of kinetically, as opposed to thermodynamically, driven self-assembly.

Surprisingly, application of a negative voltage (−0.3 V) during the self-assembly of M also resulted in a noticeable augmentation of D_M (Figure 6b). This effect is likely to be connected to the attraction of positively charged edges of montmorillonite platelets to the electrode and corresponding tilting of adsorbed platelets.

4. Surface Roughness and Defects. The effect of applying a potential during the self-assembly of P manifests itself not only in thickness but also in roughness changes. Changes in the surface roughness were assessed by SPS, AFM, and X-ray diffraction measurements.

Analysis of SPS can provide information on the surface roughness of the $(P/M)_n$ films. In the simplest case, surface plasmon resonance on a rough surface is considered to be a superimposition of two SPS curves each representing a slightly different thickness. The contribution of each curve to the experimental one is proportional to the area of the film elevated above the gold layer to this particular height. The net result is an increase of the light intensity in the minimum of the SPS curve.[47] Importantly, for nonlight-absorbing films irregularities of layer thicknesses is the only source of the increased minimum of the SPS curves. This approach was employed to describe the effect of applied potential during the self-assembly of P (Figure 8). Application of a positive +0.6 V (vs SCE) potential during the self-assembly of P in $(P/M)_n$ sandwich layers consistently elevated the minimum reflected intensity. The average thickness of the polymer layer was $D_P = 1.8 \pm 0.6$ nm, while $D_M = 2.2 \pm 0.5$ nm and $D_{P/M} = 4.0 \pm 0.5$ nm. When compared to the conditions without any external bias, it can be noted that the thickness of the polymer layer has increased slightly and so did the total thickness of each strata. However, the most important changes have been observed in the roughness of the films assembled under different conditions. While deposition of 10 sandwich layers, $(P/M)_{10}$ without potential resulted in virtually no change of the surface roughness as detected by SPS, the application of a positive voltage drastically increased it. The outcome of applying +0.6 V (vs SCE) potential during the self-assembly of P was found to depend on the number of P/M units assembled. Roughness of the $(P/M)_6$ film, *ca.* 4.9 nm, quickly increased to 5.6 and 8.7 nm for $(P/M)_{11}$ and $(P/M)_{18}$ films. The values of the surface roughness, as detemined by SPS, coincided with those observed by AFM (see the histograms in Figure 9b).

(46) Ahmadi, M. F.; Rusling, J. F. *Langmuir* **1995**, *11*, 94−100. Okahata, Y.; Shimizu, A. *Langmuir* **1989**, 5, 954−959. Hu, N.; Rusling, J. F. *Anal. Chem.* **1991**, *63*, 2163−2168. Zhang, H.; Rusling, J. F. *Talanta* **1993**, *40*, 741−747. Allara, D. L.; Parikh, A. N.; Sheshadri, K.; Craighead, H. G.; Lercel, M.; St. John, P. Abstract 50A, 70th Colloid and Surface Science Symposium; Clarkson University: Potsdam, NY, June 16−19, 1996; p 132.

(47) Due to space constraints a detailed consideration of the roughness effect on SPS curves will be published elsewhere. Here we shall only make use of the most essential results.

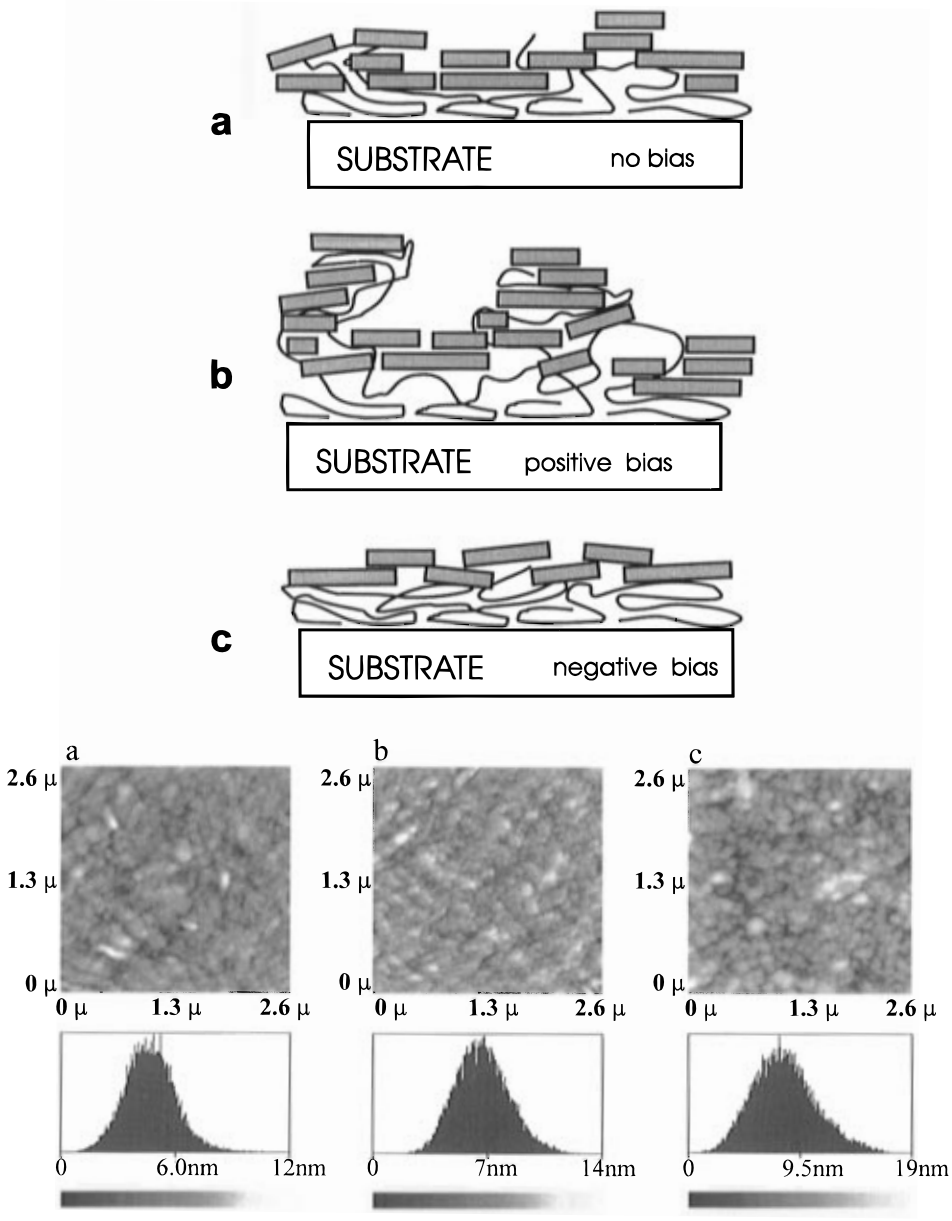

Figure 9. (a) A simplified representation of external potential effects during the self-assemply of P on the film structure. Application of positive potential (b) repulses loose parts of the polymer chain resulting in the increased disorganization and roughness of the subsequent layers of M self-assembled as compared to those assembled in the absence of an applied potential (a). The application of a negative potential results in improved morphology and denser packing of P (c). (b) Histograms of 2.6 μm $\times$ 2.6 μm AFM images obtained for a $(P/M)_6$ film (a), a $(P/M)_{11}$ film (b), and a $(P/M)_{18}$ film (c) self-assembled under the application of +0.6 V during the self-assembly of P. Samples were identical to those presented in Figure 5.

Application of a negative potential (−2.0 V, vs SCE) during the self-assembly of P in $(P/M)_n$ improved the uniformity and regularity of all deposited layers (Figure 5c). The film was exceptionally smooth, and no increase of minimum light intensity was observed even after 20 deposited layers. The mean thickness was found to be 1.0 ± 0.2, 2.6 ± 0.3, and 3.7 ± 0.1 nm for P, M, and (P/M), respectively. The thickness of the polyelectrolyte layer decreased by 40% as compared to other instances, while that of clay layer slightly increased by 18%.

Considering the effect of the external bias on the polyelectrolyte adsorption one has to take into account the existence of both tightly bound to the surface of M parts of polyelectrolyte molecules and rather loose loops and ends forming the upper part of the polymer 1−2 nm layer. Positively charged electrode surface causes repulsion of these parts of the polymer layer. Consequently, the increase of both layer thickness and layer roughness can be observed. The oppositely charged substrate surface causes strong attraction of the loose parts which results in apparent thinning of the P layer and improved regularity (Figure 10).

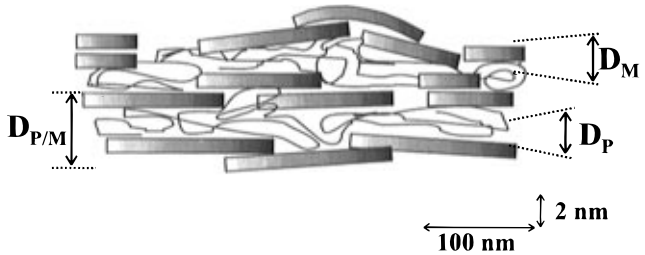

Figure 10. An oversimplified representation of a (P/M) layer: $D_{(P/M)}$ = the mean repeating distance of a (P/M) layer, D_M = the mean thickness of an M layer, and D_P = the mean thickness of a P layer.

It is important to note that the effect of applied potential is inherently kinetic in nature. The conformation of the polyelectrolyte chains attained under potential returns to the equilibrium

state in 15−20 min. This time can be extended or shortened depending on the flexibility of the polyelectrolyte, molecular weight, and the quality of a solvent (water). Drying between rinsing and adsorption of clay particles is likely to affect the conformational changes; however, complete annealing is expected to take place only when the film is immersed in solution.

The specular and off-specular reflectivity data reveal significant detail concerning subtler aspects of the film structure.[28] The presence of the 001, 003, and 004 montmorillonite basal spacing reflections along the substrate normal (Figure 3) indicate that these particles are well aligned with the substrate surface. This is not unexpected owing to the large aspect ratio of the clay sheets. The rocking curves across the 001 peak yield an average FWHM for the specular reflectivity of 0.1° which corresponds to the average angular mosaic of the normal axes associated with the clay sheets. In contrast, the FWHM of the broad, off-specular background of the rocking curves is inversely proportional to the in-plane roughness correlation length. For these films this length is extremely small (<50 nm) implying little or no roughness correlation between adjacent montmorillonite particles, i.e., adjacent clay particles do not form a coherent layer.[48]

A direct comparison of the q_z dependence for the specular ($q_x = 0$) and off-specular ($q_x \neq 0$) scattering is very revealing. In Figure 4b the peak evident at $2\Theta = 10°$ only occurs in the specular scattering, in contrast to the M peak. The diffuse scattering associated with the M sheet arises from coherent and incoherent superposition of diffuse scattering from individual particles. The lack of such diffuse scattering in the $2\Theta = 10°$ peak confirms that this feature is not associated with the clay sheets but, rather, is localized in some portion of the film. If it were a global structure incoherent scattering from the many domains within the film would result in a corresponding off-specular peak. Also, since it is along the q_z direction it is associated with a localized density modulation along the z-direction, i.e., a "layering" in some portion of the film. The width of the oscillation implies a length scale of 2.0 nm. It is most likely this represents a 2.0 nm "layer" which is adjacent to and highly correlated with the substrate. Such near-substrate layering has been seen in organic and inorganic films where the substrate interaction produces an ordered region at the substrate surface.[49] In these films such a layer most probably corresponds to the first polyelectrolyte adsorbed to the substrate surface. Similar intensity oscillations are expected at lower values of 2Θ but would be concealed by the more intense montmorillonite scattering. The ratio of the specular scattering to the diffuse scattering at $q_x = 0$ is shown in Figure 4b.[50] It decays quickly as the film thickness increases, reaching a thickness independent value between 10 and 14 layers the specular intensity is relatively constant with varying sample thickness. Rather, it is the magnitude of the diffuse scattering which mirrors the layer number. To elucidate this behavior consider the generalized scattering from a multilayer. Assuming minimal interlayer correlations the ratio of the specular to the diffuse scattering at $q_x = 0$ is given by[51,52]

$$\frac{I_{\text{specular}}}{I_{\text{diffuse}}}\Big|_{q_x=0} = \left(\int\int \mathrm{d}x\mathrm{d}y\left(e^{q_z^2 C(r_\perp^\Delta)} - 1\right)\right)^{-1} \qquad (2)$$

Here, $C(r_\perp^\Delta)$ is the in-plane roughness correlation function $\langle u(r_\perp^\Delta)u(0)\rangle$. As the magnitude of the rms roughness of the clay sheets increases the exponential term in the denominator will dominate and the overall ratio will decrease. Without detailed modeling it is impossible to determine the form of the roughness correlation function. However, since the magnitude of this ratio is inversely proportional to the rms roughness of the clay particles in the film with respect to the plane of the substrate, it can be inferred from Figure 4b that this roughness increases quickly with layer number before becoming roughly thickness independent for $N > 10$. The solid line in Figure 4b is a fit to a simple exponential decay. The good agreement is most likely fortuitous. However, it does set a decay length of approximately three layers. This is consistent with the disappearance of the Kiessig fringes in the specular scattering (shown in the insert of Figure 3) beyond $n = 7$. Thus, both specular and diffuse reflectivity data reveal a disorder of the clay particles with respect to the substrate surface which increases with an increasing layer number until a certain thickness is reached. This implies that the substrate surface acts to quench the disorder of the clay particles in the neighborhood of the surface.

The low degree of correlation between the roughness of the underlying substrate and the roughness of the P/M layer results in the formation of rather corrugated films on generally smooth surfaces. Simultaneously, being deposited on uneven surfaces $(P/M)_n$ films cause the decrease of the roughness of the underlying substrate to a level characteristic for the P/M layers. This effect can be observed by means of AFM which allows visualization the surface corrugations. The images of P/M self-assembly on etched silicon (Figures 8) probably do not require extended comments. The effect of decoupling of the roughness of the underlying substrate from the roughness of the self-assembled film is obvious. In Figure 8 one can observe that a single M platelet is sufficient to cap an etched pit of a comparable diameter. For example, this can be observed for a 188 pit in Figure 8. For a larger surface defects such as the 550 nm wide and 50 nm deep pit six P/M layers were enough to smooth up the surface. On the one hand, this effect can be perceived as the ability of P/M films to eliminate large surface defects, similarly to the gradual growth of P/M layers on hydrophobic surfaces.[53] On the other hand, it demonstrates that eventually the roughness of P/M layers is determined by the properties of its components and not by the roughness of the underlying substrate.

Conclusion

The structural hierarchy[4,54−56] renders M eminently suitable as a compartment and a template for a large variety of molecules and clusters. Species can be incorporated between the swollen layers or within the platelets of M as well as onto and/or into the surfaces and cavities of separated and/or flocculated M particles. Polymer-clay composites are considered to be an important class of hybrid advanced materials. They possess a set of unique mechanical, electrical, and gas permeation properties. This study has focused on the preparation of ordered

(48) Geer, R. E.; Shashidhar, R. *Phys. Rev. E, Rapid Commun.* **1995**, *58*, R8.

(49) Shi, Y.; Cull B.; Kumar, S. *Phys. Rev. Lett.* **1993,** *71*, 2773.

(50) The 10-layer data point in Figure 4b was not taken from a glass substrate data rather than from a film deposited on a polished Si wafer as the others.

(51) Sinha, S. K.; Sanyal, M. K.; Gibaud, A.; Satija, S. K.; Majkrzak, C. F.; Homma, H. *Science and Technology of Nanostructured Magnetic Materials*; Hadjipanayis, G. C., Prinz, G. A., Eds.; Plenum Press: New York, 1991.

(52) Geer, R. E.; Shashidhar, R.; Thibodeaux, A. F.; Duran, R. S. *Am. Phys. Soc.* **1993**, *71*, 1391−1394.

(53) Kleinfeld, E. R.; Ferguson, G. S. *Chem. Mater.* **1996**, *8*, 1575−1578.

(54) Liu, J.; Sarikaya, M.; Aksay, I. A. *Mater. Res. Soc. Symp. Proc.* **1992**, *255*, 9−17.

(55) Lakes, R. *Nature* **1993**, *361*, 511−515.

(56) Dékány, I.; Fendler, J. H. In *Fine Particles Science and Technology from Micro to Nanoparticles*; Pelizetti, E., Ed.; Kluwer Academic Publishers: The Netherlands, 1996; pp 443−455.

$(P/M)_n$ multilayer structures by using a simple self-assembly technique. Such films were found to assemble on a variety of substrates such as glass, quartz, metal, and plastic. The structure of P/M layers was elucidated by X-ray diffraction, X-ray reflectivity, atomic force microscopy, transmission electron microscopic, and surface plasmon spectroscopic measurements. The mechanism of film formation is expected to involve the following steps: first, adsorption of a P layer onto the substrate surface by electrostatic and van der Waals interactions. Upon rinsing, the loosely bound polyelectrolyte molecules are removed; however, the adsorbed layer is unlikely to be in a thermodynamic equilibrium with water. Second, the M layer adsorbs strongly and irreversibly (as confirmed by bulk precipitation studies of P and M) onto the oppositely charged polyelectrolyte layer. The irregular M sheets cannot provide a complete coverage of a P layer. They form overlapping stacks in order to cover the P chains intercalated into the M sheets. The interfacial roughness exceeds the thickness of a P/M layer. Therefore, the X-ray diffraction peak corresponding to the interplanar distance is hardly observable. The observed X-ray reflectivity peaks were attributed to the M basal spacing and to its harmonics, to Kiesseg-fringes, and to the near-substrate structuring of the P chains. Specular and off-specular diffraction data revealed very consistent planar orientation of the M sheets and showed the surface roughness to be independent of substrate used. Similar behavior was observed by *in situ* AFM measurements upon deposition of new layers on the same area. As such the M platelets were observed to cap and to smooth large surface irregularities on etched silicon surfaces. Some control over surface roughness can be obtained by the application of an external voltage during the self-assemble of P; using a negative bias produced more regular and uniform self-assembled films.

Acknowledgment. Support of this work by the National Science Foundation (J.H.F.), Hungarian Scientific Research Found, OTKA I/5 T007531, I/6 T014159, and W015313 (ID), the U.S.−Hungarian Joint Fund Pr. Nr. 227/92a (J.H.F. and I.D.), and the Hungarian Ministry of Education, MKM, Pr. Nr. 219/1995 is gratefully acknowledged. N.A.K. wants to thank all members of the Laboratory of Colloid Chemistry, Attila József University, Szeged, Hungary, for their assistance and help during his stay there. N.A.K. also acknowledges financial support from Oklahoma State University.

Supporting Information Available: Figures of X-ray diffraction patterns, X-ray patterns of solids, rocking curves at the (001) reflection of the montmorillonite particles, theoretical treatment of surface roughness imaged by SPS, proposed treatment of surface roughness, plot of absorbances vs *n* for a $(P/M)_n$ film, and AFM images (13 pages). See any current masthead page for ordering and Internet access instructions.

JA964409T